Spin-polarized supercurrent through the van der Waals Kondo-lattice ferromagnet Fe_3GeTe_2

Deepti Rana,[1] Aswini R,[1] Basavaraja G,[2] Chandan Patra,[3] Sandeep Howlader,[1] Rajeswari Roy Chowdhury,[3] Mukul Kabir,[2] Ravi P. Singh,[3] and Goutam Sheet[1,*]

[1]*Department of Physical Sciences, Indian Institute of Science Education and Research (IISER) Mohali, Sector 81, S. A. S. Nagar, Manauli, P.O. 140306, India*

[2]*Department of Physics, Indian Institute of Science Education and Research (IISER) Pune, P.O. 411008, India*

[3]*Department of Physics, Indian Institute of Science Education and Research (IISER) Bhopal, P.O. 462066, India*

(Received 5 May 2022; revised 27 June 2022; accepted 26 July 2022; published 11 August 2022)

In the new van der Waals Kondo-lattice Fe_3GeTe_2, itinerant ferromagnetism and heavy fermionic behavior coexist. Both the key properties of such a system, namely, a spin-polarized Fermi surface and a low Fermi momentum, are expected to significantly alter Andreev-reflection-dominated transport at a contact with a superconducting electrode and display unconventional proximity-induced superconductivity. We observed interplay between Andreev reflection and Kondo resonance at mesoscopic interfaces between superconducting Nb and Fe_3GeTe_2. Above the critical temperature (T_c) of Nb, the recorded differential conductance (dI/dV) spectra display a robust zero-bias anomaly which is described well by a characteristic Fano line shape arising from Kondo resonance. Below T_c, the Fano line mixes with Andreev-reflection-dominated dI/dV, leading to a dramatic, unconventional suppression of conductance at zero bias. As a consequence, an analysis of the Andreev reflection spectra within a spin-polarized model yields an anomalously large spin polarization which is not explained by the density of states of the spin-split bands at the Fermi surface alone. The results open up the possibilities of fascinating interplay between various quantum phenomena that may potentially emerge at the mesoscopic superconducting interfaces involving Kondo-lattice systems hosting spin-polarized conduction electrons.

DOI: 10.1103/PhysRevB.106.085120

I. INTRODUCTION

Spin-polarized transport characteristics through mesoscopic junctions between conventional superconductors and complex magnetic systems may display unconventional features related to exotic Fermi surface properties. In a normal metal/superconducting junction the transport is dominated by Andreev reflection [1], a quantum process through which conversion of normal current in the metal to a supercurrent in the superconductor happens. The process involves reflection of an up (down) spin electron as a down (up) spin hole, thereby causing a conductance enhancement below the superconducting energy gap. When the normal metal is an itinerant ferromagnet characterized by a spin-polarized Fermi surface, all the electrons in the Fermi surface cannot undergo Andreev reflection, as all the corresponding Andreev-reflected holes would not find states in the opposite spin band. This leads to a suppression of Andreev reflection in spin-polarized junctions. A measurement of the suppression of Andreev reflection gives an estimate of the spin polarization at the Fermi surface [2–10]. The problem gains additional complexity when the spin-polarized electrode forming the junction with a superconductor hosts significant electron correlations. In such cases, additional suppression of Andreev reflection is expected due to a larger effective potential barrier that would arise from the intrinsic mismatch in the Fermi velocities in the two sides of the junction [11]. The situation approaches an extreme limit when the carriers in the spin-polarized part of the junction are also characterized by a large effective mass as in the heavy fermions. In such cases, the suppression of conductance may not be only due to spin polarization and larger potential barrier, both of which can be modeled within an appropriately modified version of the conventional Blonder-Tinkham-Klapwijk (BTK) theory [2].

The transport spectroscopic features in the aforementioned situations may also involve signature of other electronic effects in various forms, including a Kondo anomaly [12–15]. Within the theory of electron tunneling into a Kondo lattice [16] (as in case of a point-contact geometry), it was earlier shown that a cotunneling mechanism causes spin-flip processes. In the presence of that, the calculation of the conductance within a mean-field picture predicts the appearance of two peaks separated by a hybridization gap in the clean limit, which gets smeared out as one approaches the dirty (disordered) limit. Within this picture, even with moderate disorder the conductance spectrum is expected to take the shape of a Fano line [17]. Such Fano line-shape behaviors were experimentally observed in point contacts with a number of heavy fermion systems in the past [12–15].

In addition to the above, other complex possibilities may also arise. For example, the superconducting phase induced (proximity) in the heavy fermionic part of the junction may achieve unconventional character in the order parameter symmetry. While such possibilities were explored experimentally in nonmagnetic or weakly magnetic heavy fermion superconductors like $CeCoIn_5$ [12], $CeCu_2Si_2$, URu_2Si_2 [18], UBe_{13}, UPt_3 [19], UTe_2 [20], etc., investigation of such phenomena in a ferromagnetic Kondo lattice with heavy fermionic character

*goutam@iisermohali.ac.in

was not investigated, mainly due to lack of a model system where all such physical properties would coexist.

Recently it was shown that the van der Waals (vdW) ferromagnet Fe_3GeTe_2 hosts Fermi-surface spin polarization, an emergent Kondo-lattice behavior, along with a large carrier mass leading to a heavy fermion character to the system [21,22]. Bulk crystalline Fe_3GeTe_2 is a van der Waals layered material that crystallizes into a hexagonal lattice structure with space group $P6_3/mmc$ [23,24], as shown in Fig. 1(a). The Fe atoms occupy two inequivalent Wyckoff positions denoted as Fe-I and Fe-II. The Fe-II atoms are covalently bonded with Ge at the middle layer, which is sandwiched between two hexagonal layers of Fe-I. This triple-layer Fe_3Ge are further sandwiched between two hexagonal Te layers, and a vdW gap separates the resultant pentuple layers Fe_3GeTe_2. Unlike other bulk vdW ferromagnets CrI_3 [25] and $CrSiTe_3$ [26], it is an itinerant ferromagnet with high Curie temperature of 220–230 K [23,24], which can be further increased by doping [27] or patterning [28], making it a promising candidate for next-generation spintronic devices [29–31]. The system shows a planar topological Hall effect [32], along with significantly high uniaxial magnetic anisotropy [33–36]. The existence of strong correlations in Fe_3GeTe_2 is concluded from evidences of enhanced specific heat described by a high Sommerfeld coefficient pointing to a ($\sim$ tenfold) mass enhancement [37]. In this work, we have performed Andreev reflection spectroscopy at point-contact junctions between tips of superconducting Nb and single crystals of the Kondo-lattice ferromagnet Fe_3GeTe_2.

II. MAGNETIC FORCE MICROSCOPY ON Fe_3GeTe_2

High-quality single crystals of Fe_3GeTe_2 were synthesized by chemical vapor transport. The details of the growth parameters and the characterization are reported elsewhere [38]. Owing to the van der Waals bonding between the different layers, the single crystals were cleavable by mechanical exfoliation. We exposed the fresh surface of the crystals before transferring them to the cryogenic measurement stages.

Magnetization measurements revealed a critical temperature of $\sim$206 K [38]. In order to investigate the local magnetic properties, we imaged the ferromagnetic domains of Fe_3GeTe_2 directly by low-temperature magnetic force microscopy. At the lowest temperature, in the absence of any external magnetic field treatment we found clear stripe domains with a typical stripe width of $\sim$700 nm [Fig. 1(b)]. The stripe domains in a large-size crystal are a consequence of strong uniaxial anisotropy, as is usually reported for Fe_3GeTe_2 from bulk magnetization measurements [33,39,40]. The stripe domains also form interconnects closely resembling the domain structures that are theoretically expected for the zero-field treated states of skyrmionic systems. We have also performed field-cooled measurements to investigate the skyrmion physics in the system, but a discussion of that is beyond the scope of this paper. The temperature evolution of the ferromagnetic domains is presented in Figs. 1(b)–1(f). The width of the stripe domains increases with increase in temperature and disappears at 205 K, near the Curie temperature. In the temperature range over which Andreev reflection experiments discussed below were performed, no significant

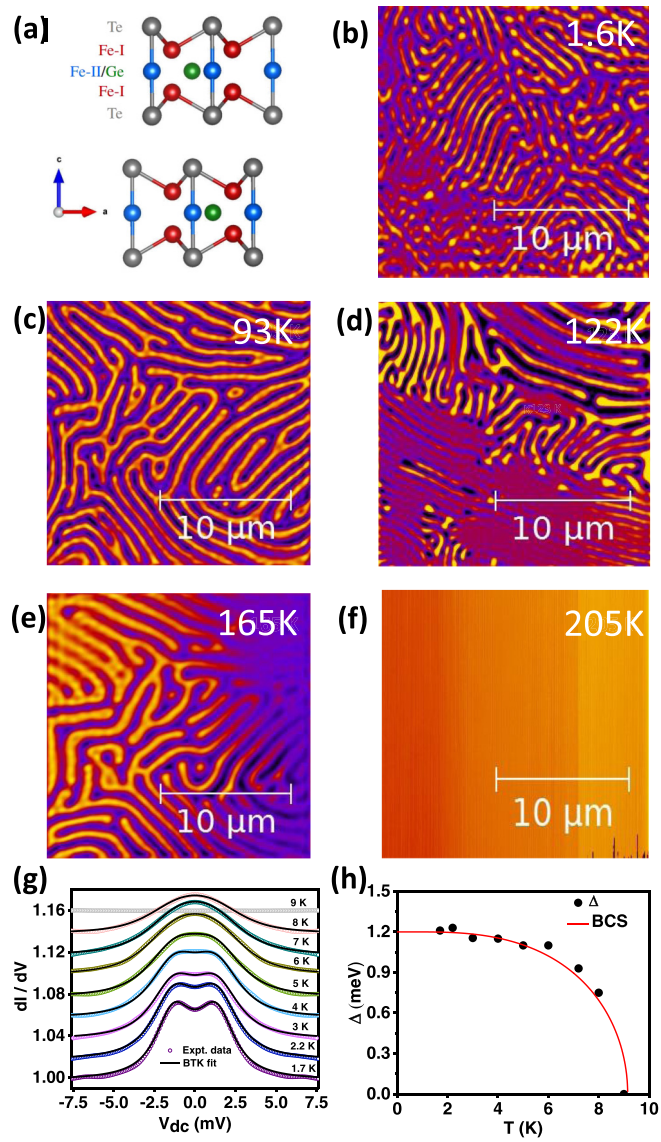

FIG. 1. (a) Crystal structure of Fe_3GeTe_2. (b)–(f) Magnetic force microscopy (MFM) dual-pass-phase images of Fe_3GeTe_2, at different temperatures, showing contrast of ferromagnetic domains. The scale bar is 10 μm. The stripe domains vanishes as temperature is raised to 205 K. (g) Temperature dependence of ballistic spectra (shown by colored dots) and their corresponding BTK fits (shown by black line). All the spectra are normalized, and an equal vertical shift to spectra with respect to the conductance spectrum at 1.7 K is given for clarity. (h) Temperature dependence of the superconducting gap (shown by black dots). The expected variation of the gap from BCS theory is shown by a solid red line.

change in the domain structure/size was seen. As we discuss below, statistically, the large domain size enabled the Nb tips to engage on individual domains for spin-polarization measurements through Andreev reflection.

III. POINT CONTACT SPECTROSCOPY AT Nb/Fe_3GeTe_2 JUNCTIONS

For the Andreev reflection spectroscopy experiments, an Nb tip was engaged by the standard needle-anvil method on a

freshly cleaved single crystal of Fe_3GeTe_2 inside a variable-temperature cryostat working down to 1.4 K which is also equipped with a three-axis superconducting vector magnet (6T-1T-1T). The point contacts were formed on the [001] facet such that the current was injected along the c axis of the crystal. For this direction of current injection, the layered structure does not play a role in deciding the point-contact resistance and its microscopic anatomy. Owing to the high quality of the single crystals, the ballistic superconducting point contacts, characterized by two differential conductance (dI/dV) peaks symmetric about $V = 0$, could be established fairly easily. One such representative spectrum and its temperature dependence is shown in Fig. 1(g). The colored points are experimentally obtained data points at different temperatures, and the solid black lines are the corresponding fits within a modified BTK theory [2], modified to incorporate the effect of the spin-polarized band structure of the ferromagnetic fraction of the point contacts.

In a normal metal-superconductor Andreev reflection process, the zero-bias conductance should be two times the normal-state conductance for a fully transparent barrier and at absolute zero [41]. While finite temperature broadens the spectral features with marginal reduction of dI/dV at $T < 0.5T_c$, a nonzero interfacial barrier ($Z \neq 0$) causes suppression of the zero-bias conductance in a characteristic way that also causes enhancements (sharpening) of the dI/dV peaks near $V = \pm\Delta/e$. However, with a visual inspection of the spectra presented in Fig. 1(g), it is clear that the barrier is transparent (low Z), despite that Andreev reflection has been suppressed significantly. The zero-bias enhancement is only about 6%. The spectrum could be described well within the modified BTK theory with an effective spin polarization (P_t) of 46.57%, but only with an enhanced effective temperature of 4.6 K, or a rather large (Dynes like [42]) broadening parameter (Γ) approaching 0.52 meV, which is almost 0.5Δ. The need of a significantly enhanced effective temperature, or, instead, a larger Γ, is due to additional broadening effects that could be playing a role here but the origin of which is unclear. We note that this effect is not due to contact heating because the normal-state resistance did not change with increasing temperature, no additional spectral features other than the double-peak structure were seen, and Wexler's formula [43] gave an estimate of the contact diameter ~20 nm, which is smaller than the mean free path in Fe_3GeTe_2, thereby confirming that the contacts are ballistic and no significant contact heating is expected. Since the contact diameter is smaller than the domain size, statistically, the majority of the times, the point contacts are formed on single domains. Furthermore, taking the measured temperature as the contact temperature, the Δ vs T graph is well described by the Bardeen-Cooper-Schrieffer (BCS) theory [44] [solid red line in Fig. 1(h)]. It should be noted that a significant Δ is found even at measured $T = 8$ K, and any significant contact heating would make the contact nonsuperconducting at a much lower temperature. Furthermore, a larger effective temperature should also lead to an underestimation of P_t. There is also a possibility that certain local disorders under the point contacts give rise to the additional broadening. The point contacts were made on the freshly cleaved surfaces of single-crystalline Fe_3GeTe_2. Hence the possibility of such a

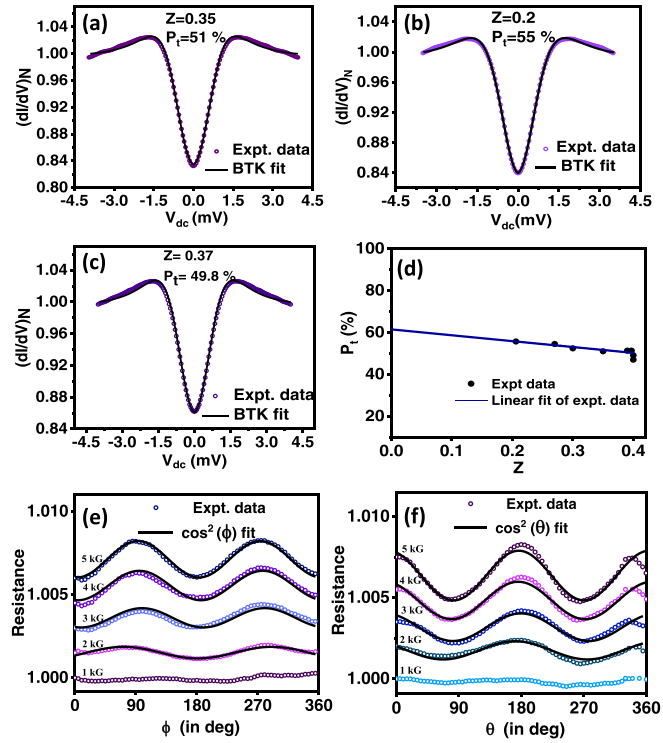

FIG. 2. (a)–(c) Three fitted ballistic spectra with different values of barrier strength (Z) and spin polarization (P_t). (d) P_t vs Z. The extrapolated value of P_t (at $Z = 0$) is around 61%. (e), (f) In-plane and out-of plane magnetic field-angle dependence of resistance taken at zero bias and 11 K. The $\cos^2(\phi)$ and $\cos^2(\theta)$ fits are shown by solid black lines. All the resistance curves are normalized, and an equal vertical shift to resistance curves with respect to the curve at the lowest magnetic field is given for clarity.

effect should be low—though that cannot be completely ruled out.

As per the standard practice, the intrinsic spin polarization can be estimated by performing experiments with a number of spectra for junctions with different barrier strengths (Z) and then extrapolating the Z dependence of P_t to $Z = 0$. We investigated several other point contacts which display features of a higher Z. We show three such representative spectra, along with their modified BTK fits in Figs. 2(a)–2(c). P_t was seen to monotonically decrease with increasing Z, and the extrapolated dependence to $Z = 0$ revealed a spin polarization greater than 60%, as shown in Fig. 2(d). In all these cases, however, the effective temperature (or, the artificially introduced Dyne's-like broadening parameter Γ) used for the analysis was significantly high, indicating that the intrinsic Fermi-surface spin polarization could be even higher.

Here we would also like to highlight that the point contact showed strong anisotropy in magnetoresistance. To investigate that, we performed field-angle dependence of the normal-state resistance of one such ballistic point contact at zero bias. The orientation of the magnetic field with respect to the applied current was varied using the three-axis vector magnet. The results for in-plane rotation (ϕ) of field and out-of-plane rotation (θ) of the magnetic field are shown in Figs. 2(e) and 2(f), respectively. The anisotropy in magne-

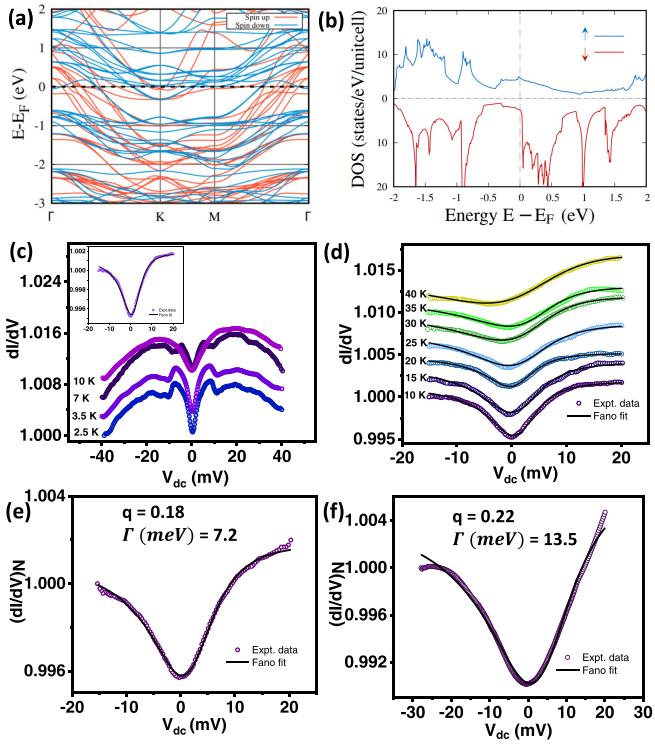

FIG. 3. (a), (b) Band structure and the electronic density of states (DOS) is calculated for the ferromagnetic state, respectively. (c) The temperature dependence of high-Z point contact. The inset shows the Fano line-shape fitting (shown by black line) of the conductance spectrum (shown by colored dots) taken at 10 K. (d) Temperature dependence of the normal state along with the Fano line-shape fits. Spectra are vertically shifted for clarity. (e), (f) Three normalized conductance spectra (shown by colored dots) and their Fano line-shape fitting (shown by black line) taken at 12 K.

toresistance became more pronounced with increase in the strength of the field. The anisotropic behavior followed typical $\cos^2(\phi)$ and $\cos^2(\theta)$ dependence [shown by the black lines in the Figs. 2(e)–2(f)], signifying the spin-polarized nature [8] of the transport supercurrent flowing through the Nb/Fe_3GeTe_2 point contacts.

IV. BAND-STRUCTURE CALCULATIONS AND ANALYSIS

In order to gain insight on the spin-polarized Fermi surface of Fe_3GeTe_2, we performed first-principles density functional calculations. We have presented the detailed calculated band structures in Fig. 3(a). We focus on the key features of the calculated band structure here. The spin-polarized electronic structure analysis indicates the metallic nature of Fe_3GeTe_2, which along with the noninteger magnetic moment, supports the itinerant nature of ferromagnetism. The appearance of several flat bands near the Fermi level indicates enhanced quasiparticle mass, suggesting a strong electron correlation in the material. This is in agreement with the high Sommerfeld coefficient of specific heat data published in the past [37]. The states at the Fermi level are constructed with d_{yz} and d_{xz} orbitals from Fe-I hybridized with the Te-p orbitals for the majority spin channel. In addition, a contribution from the d_{xy} from Fe-II is also observed but is significantly lower. Similar trends are encountered for the minority spin channel. To note, the band structure of the system was also calculated earlier [21], though not in the context of the Fermi-level spin polarization. The key aspects of our calculations are consistent with the past calculations. We have used the calculated bands to extract additional parameters for the analysis of our experimental data. In general, as far as the transport measurements are concerned, the general expression for (transport) spin polarization can be written as [45]

$$P_t^n = \frac{\langle N(E_F) v_F^n \rangle_\uparrow - \langle N(E_F) v_F^n \rangle_\downarrow}{\langle N(E_F) v_F^n \rangle_\uparrow + \langle N(E_F) v_F^n \rangle_\downarrow}, \quad (1)$$

where v_F is the spin-polarized Fermi velocity. The Fermi velocity of the individual bands can be calculated from the slope of the individual bands at the Fermi energy. Taking the arithmetic average of the velocities of all the bands results in the average Fermi velocity for the respective spin channels. $n = 0$ gives the net Fermi-surface spin polarization, which is not the relevant quantity here, as the Fermi velocity of the up- and the down-spin channels can be different too. In point-contact spectroscopy, $n = 1$ and $n = 2$ give P_t in the ballistic and diffusive regimes, respectively. From our calculations, we found the average Fermi velocity of the majority spin channel to be $v_{F\uparrow} = 4.10 \times 10^5\ \mathrm{ms}^{-1}$, which is larger than the minority spin channel, $v_{F\downarrow} = 2.86 \times 10^5\ \mathrm{ms}^{-1}$. The observation of Fermi velocities an order of magnitude slower than that in the typical metals is consistent with the reported higher fermion mass in the system. The calculated spin-polarized density of states at the Fermi level is $N_\uparrow = 4.72$ states/eV/unit cell, that is 79% greater than $N_\downarrow$ [Fig. 3(b)]. Therefore the imbalance of both v_F and $N(E_F)$ result in the transport spin polarization of 44% in the ballistic regime and 58% in the diffusive regime. To note, these estimates were done at absolute zero temperature and did not involve the effects of thermal broadening at the measurement temperatures. In principle, the measured spin polarization should be significantly smaller than the theoretically obtained numbers. However, the experimentally measured spin polarization was found to be higher even with larger effective temperatures [or higher effective broadening parameters (Γ)].

V. KONDO-LATTICE BEHAVIOR

The above observation motivated us to investigate the possibility of any other physics competing and/or cooperating with spin-polarized Andreev reflection at the Nb/Fe_3GeTe_2 interfaces. For that, we gradually increased the temperature of the point contact for a high Z contact, as shown in Fig. 3(c), and noted the spectral features over a larger bias range (± 40 mV). As it was mentioned before, the central dip in an Andreev reflection spectrum is primarily due to nonzero Z and P_t, and that should disappear at the T_c of the superconductor forming the junction. However, we found that the central dip structure remained even above 10 K, definitely above the T_c of Nb. Moreover, the normal-state spectra also displayed broad conductance peaks at around ± 18 mV. These peaks compete with the Andreev reflection features in the superconducting state, thereby causing anomalous features

near 15 mV, where the background gives a downward trend to dI/dV with decreasing V, while the peaks due to Andreev reflection give an upward trend. It is this competition that brings the zero-bias conductance of the 10-K spectrum below the 7-K spectrum. In this context, we note that the relative strength of the background anomaly and the enhancement due to Andreev reflection are seen to be different at different points. A visual inspection of the spectra presented in Fig. 3(c), and Figs. 2(a)–2(c) clearly reveal this difference.

Now it is important to understand the special features in dI/dV that appeared above the T_c of Nb. A careful inspection of the normal-state data reveals an asymmetry between the $\pm V$ regions. As shown in the inset of Fig. 3(c), the asymmetry observed in our data at 10 K could be fit well with a Fano line shape [17]. The line shape was generated using the formula

$$dI/dV \propto \frac{(\epsilon + q)^2}{1 + \epsilon^2}; \quad \epsilon = \frac{eV - \epsilon_0}{\gamma}. \tag{2}$$

Here, V is the dc bias, q is the asymmetry factor, ϵ_0 is the position of the resonance in the energy scale, and γ is the resonance at HWHM (half width at half maximum). Since a Kondo-lattice behavior has already been reported in Fe_3GeTe_2 [21,22], it is rational to attribute the Fano-like normal-state feature with Kondo effect in a Kondo lattice. The normal state of various ballistic contacts was investigated, and two such normal-state spectra along with Fano fitting parameters are shown in Figs. 3(e)–3(f). For a Kondo lattice like Fe_3GeTe_2, under a point-contact geometry, within a two-channel model, the special line shape might be due to the interference between the two current paths, one through the channel of the itinerant electrons and the other one through the quasiparticles that have attained a significantly higher mass due to the interaction between the d-electron spins and the spins of the itinerant electrons. In Fig. 3(d), we investigated the normal-state spectra and their Fano line shape as a function of increasing temperature. The resonance width given by γ increases with increasing temperature. This behavior is commonly seen in Kondo-induced Fano line shapes of dI/dV spectra. Such Fano line-shape fitting of experimental point-contact spectra was also done for a number of heavy fermionic superconductors in the past, including $CeCoIn_5$ [12,13] and URu_2Si_2 [14].

VI. CONCLUSION

Therefore, from the analysis of the superconducting and the normal-state spectra, it is understood that the Andreev reflection features appear in the presence of a strong background due to the Kondo-lattice behavior of Fe_3GeTe_2. The Kondo-related features interplay with the superconductivity-related features below the T_c of Nb. Since the Kondo anomaly at zero bias contributes to the overall conductance drop at $V = 0$, a modified BTK fit without incorporating Kondo effect is expected to give an overestimate of P_t. In other words, an enhanced P_t needs to be used to take into account the additional suppression of the low-bias Andreev reflection due to the presence of the Kondo-lattice background. This explains the apparent discrepancy between the experimentally measured parameters with the estimates using the band-structure calculations.

ACKNOWLEDGMENTS

D.R. thanks DST INSPIRE for financial support. G.S. acknowledges financial support from a Swarnajayanti Fellowship awarded by the Department of Science and Technology, Government of India (Grant No. DST/SJF/PSA-01/2015-16).

[1] A. F. Andreev, Zh. Eksp. Teor. Fiz. **46**, 1823 (1964) [Sov. Phys. JETP **19**, 1228 (1964)].
[2] R. J. Soulen, Jr., M. S. Osofsky, B. Nadgorny, T. Ambrose, P. Broussard, and S. F. Cheng, J. Appl. Phys. **85**, 4589 (1999).
[3] M. J. M. de Jong and C. W. J. Beenakker, Phys. Rev. Lett. **74**, 1657 (1995).
[4] S. K. Upadhyay, A. Palanisami, R. N. Louie, and R. A. Buhrman, Phys. Rev. Lett. **81**, 3247 (1998).
[5] N. Auth, G. Jakob, T. Block, and C. Felser, Phys. Rev. B **68**, 024403 (2003).
[6] S. Howlader, S. Saha, R. Kumar, V. Nagpal, S. Patnaik, T. Das, and G. Sheet, Phys. Rev. B **102**, 104434 (2020).
[7] S. Kamboj, S. Das, A. Sirohi, R. R. Chowdhury, S. Gayen, V. K. Maurya, S. Patnaik, and G. Sheet, J. Phys.: Condens. Matter **30**, 355001 (2018).
[8] L. Aggarwal, S. Gayen, S. Das, R. Kumar, V. Su, C. Felser, C. Shekhar, and G. Sheet, Nat. Commun. **8**, 13974 (2017).
[9] A. Sirohi, C. K. Singh, G. S. Thakur, P. Saha, S. Gayen, A. Gaurav, S. Jyotsna, Z. Haque, L. C. Gupta, M. Kabir, A. K. Ganguli, and G. Sheet, Appl. Phys. Lett. **108**, 242411 (2016).
[10] S. Mukhopadhyay, P. Raychaudhuri, D. A. Joshi, and C. V. Tomy, Phys. Rev. B **75**, 014504 (2007).
[11] E. Tuuli and K. Gloos, Low Temp. Phys. **37**, 485 (2011).
[12] W. K. Park, J. L. Sarrao, J. D. Thompson, and L. H. Greene, Phys. Rev. Lett. **100**, 177001 (2008).
[13] M. Fogelström, W. K. Park, L. H. Greene, G. Goll, and M. J. Graf, Phys. Rev. B **82**, 014527 (2010).
[14] W. K. Park, P. H. Tobash, F. Ronning, E. D. Bauer, J. L. Sarrao, J. D. Thompson, and L. H. Greene, Phys. Rev. Lett. **108**, 246403 (2012).
[15] Y.-F. Yang, Phys. Rev. B **79**, 241107(R) (2009).
[16] M. Maltseva, M. Dzero, and P. Coleman, Phys. Rev. Lett. **103**, 206402 (2009).
[17] U. Fano, Phys. Rev. **124**, 1866 (1961).
[18] Y. De Wilde, J. Heil, A. G. M. Jansen, P. Wyder, R. Deltour, W. Assmus, A. Menovsky, W. Sun, and L. Taillefer, Phys. Rev. Lett. **72**, 2278 (1994).
[19] A. Nowack, A. Heinz, F. Oster, D. Wohlleben, G. Güntherodt, Z. Fisk, and A. Menovsky, Phys. Rev. B **36**, 2436(R) (1987).
[20] L. Jiao, S. Howard, S. Ran, Z. Wang, J. O. Rodriguez, M. Sigrist, Z. Wang, N. P. Butch, and V. Madhavan, Nature (London) **579**, 523 (2020).

[21] Y. Zhang, H. Lu, X. Zhu, S. Tan, W. Feng, Q. Liu, W. Zhang, Q. Chen, Y. Liu, X. Luo, D. Xie, L. Luo, Z. Zhang, and X. Lai, Sci. Adv. **4**, eaao6791 (2018).
[22] M. Zhao, B.-B. Chen, Y. Xi, Y. Zhao, H. Xu, H. Zhang, N. Cheng, H. Feng, J. Zhuang, F. Pan, X. Xu, W. Hao, W. Li, S. Zhou, S. X. Dou, and Y. Du, Nano Lett. **21**, 6117 (2021).
[23] H.-J. Deiseroth, K. Aleksandrov, C. Reiner, L. Kienle, and R. K. Kremer, Eur. J. Inorg. Chem. **2006**, 1561 (2006).
[24] B. Chen, J. Yang, H. Wang, M. Imai, H. Ohta, C. Michioka, K. Yoshimura, and M. Fang, J. Phys. Soc. Jpn. **82**, 124711 (2013).
[25] B. Huang, G. Clark, E. Navarro-Moratalla, D. R. Klein, R. Cheng, K. L. Seyler, D. Zhong, E. Schmidgall, M. A. McGuire, D. H. Cobden, W. Yao, D. Xiao, P. Jarillo-Herrero, and X. Xu, Nature (London) **546**, 270 (2017).
[26] M.-W. Lin, H. L. Zhuang, J. Yan, T. Z. Ward, A. A. Puretzky, C. M. Rouleau, Z. Gai, L. Liang, V. Meunier, B. G. Sumpter, P. Ganesh, P. R. C. Kent, D. B. Geohegan, D. G. Mandrusbc, and K. Xiao, J. Mater. Chem. C **4**, 315 (2016).
[27] Y. Deng, Y. Yu, Y. Song, J. Zhang, N. Z. Wang, Z. Sun, Y. Yi, Y. Z. Wu, S. Wu, J. Zhu, J. Wang, X. H. Chen, and Y. Zhang, Nature (London) **563**, 94-99 (2018).
[28] Q. Li, M. Yang, C. Gong, R. V. Chopdekar, A. T. N'Diaye, J. Turner, G. Chen, A. Scholl, P. Shafer, E. Arenholz, A. K. Schmid, S. Wang, K. Liu, N. Gao, A. S. Admasu, S. W Cheong, C. Hwang, J. Li, F. Wang, X. Zhang, and Z. Qiu, Nano Lett. **18**, 5974 (2018).
[29] K. S. Burch, D. Mandrus, and J.-G. Park, Nature (London) **563**, 47 (2018).
[30] K. F. Mak, J. Shan, and D. C. Ralph, Nat. Rev. Phys. **1**, 646 (2019).
[31] C. Gong and X. Zhang, Science **363**, eaav4450 (2019).
[32] Y. You, Y. Gong, H. Li, Z. Li, M. Zhu, J. Tang, E. Liu, Y. Yao, G. Xu, F. Xu, and W. Wang, Phys. Rev. B **100**, 134441 (2019).
[33] N. León-Brito, E. D. Bauer, F. Ronning, J. D. Thompson, and R. Movshovicha, J. Appl. Phys. **120**, 083903 (2016).
[34] H. L. Zhuang, P. R. C. Kent, and R. G. Hennig, Phys. Rev. B **93**, 134407 (2016).
[35] V. Yu. Verchenko, A. A. Tsirlin, A. V. Sobolev, I. A. Presniakov, and A. V. Shevelkov, Inorg. Chem. **54**, 8598 (2015).
[36] B. Chen, J.-H. Yang, H. Ohta, C. Michioka, and K. Yoshimura, J. Jpn. Soc. Powder Metall. **57**, 172 (2010).
[37] J.-X. Zhu, M. Janoschek, D. S. Chaves, J. C. Cezar, T. Durakiewicz, F. Ronning, Y. Sassa, M. Mansson, B. L. Scott, N. Wakeham, E. D. Bauer, and J. D. Thompson, Phys. Rev. B **93**, 144404 (2016).
[38] R. R. Chowdhury, S. DuttaGupta, C. Patra, O. A. Tretiakov, S. Sharma, S. Fukami, H. Ohno, and R. P. Singh, Sci. Rep. **11**, 14121 (2021).
[39] L. Cai, C. Yu, L. Liu, W. Xia, H.-A. Zhou, L. Zhao, Y. Dong, T. Xu, Z. Wang, Y. Guo, Y. Zhao, J. Zhang, L. Yang, L. Yang, and W. Jiang, Appl. Phys. Lett. **117**, 192401 (2020).
[40] H. Wang, C. Wang, Z.-A. Li, H. Tian, Y. Shi, H. Yang, and J. Li, Appl. Phys. Lett. **116**, 192403 (2020).
[41] G. E. Blonder, M. Tinkham, and T. M. Klapwijk, Phys. Rev. B **25**, 4515 (1982).
[42] R. C. Dynes, V. Narayanamurti, and J. P. Garno, Phys. Rev. Lett. **41**, 1509 (1978).
[43] A. Wexler, Proc. Phys. Soc. **89**, 927 (1966).
[44] J. Bardeen, L. N. Cooper, and J. R. Schrieffer, Phys. Rev. **108**, 1175 (1957).
[45] I. I. Mazin, Phys. Rev. Lett. **83**, 1427 (1999).